Optimizing magnetic heating of isolated magnetic nanowires (MNWs) by simulation

Cite as: AIP Advances 12, 035007 (2022); https://doi.org/10.1063/9.0000335 Submitted: 01 November 2021 • Accepted: 04 November 2021 • Published Online: 03 March 2022

in Yicong Chen, Allison Harpel and Bethanie J. Hills Stadler













ARTICLE AIP Advances scitation.org/journal/adv

Optimizing magnetic heating of isolated magnetic nanowires (MNWs) by simulation

Cite as: AIP Advances 12, 035007 (2022); doi: 10.1063/9.0000335 Presented: 27 December 2021 • Submitted: 1 November 2021 • Accepted: 4 November 2021 • Published Online: 3 March 2022







Yicong Chen, Delison Harpel, and Bethanie J. Hills Stadler

AFFILIATIONS

Department of Electrical and Computer Engineering, University of Minnesota, Twin Cities 200 Union Street SE, Minneapolis, Minnesota 55455, USA

Note: This paper was presented at the 15th Joint MMM-Intermag Conference. a) Author to whom correspondence should be addressed: chen6587@umn.edu

ABSTRACT

Magnetic properties such as coercivity, remanence and saturation magnetization will determine the area enclosed by the hysteresis loop of a magnetic material, which also represents magnetic heating. Nanowarming of cryopreserved organs is a new application for magnetic heating using nanoparticles. In this paper, isolated Ni MNW of different sizes and shapes are studied via micromagnetic simulation to explore the optimization of heating using individual MNW. Ellipsoidal MNWs with small (30nm) diameters turn out to be most promising in heating ability due to their large hysteresis area and their potential to distribute uniformly in an organ that is being heated. In addition to optimized heating, a special switching pattern of magnetic moment was also observed for cylindrical large (200nm) MNW. This special switching pattern can trigger applications such as quantum computing.

© 2022 Author(s). All article content, except where otherwise noted, is licensed under a Creative Commons Attribution (CC BY) license (http://creativecommons.org/licenses/by/4.0/). https://doi.org/10.1063/9.0000335

INTRODUCTION

A magnetic nanowire (MNW) is a type of material with special 1D structure. The diameter of the material is in nanoscale and the length can range from nanometers to hundreds of microns. MNWs are usually fabricated via electrodeposition with the help of porous template such as anode aluminum oxide (AAO) and track-etched polycarbonate (TEPC). By applying techniques such as pulse-plating and multiple electrolyte bath, layered MNWs with different materials can be fabricated. As compared with bulk magnetic materials, nanoscale MNWs bear unique magnetic properties due to their large shape anisotropy. The magnetic properties are typically measured in the form of hysteresis loops where the magnetization is plotted vs an applied magnetic field. From the hysteresis loop, many essential magnetic properties such as the coercivity and remanence can be revealed. By controlling these magnetic properties, the MNWs can be studied and applied in a variety of technical areas. Segmented MNWs show giant magnetoresistance (GMR).²⁻⁴ This discovery triggered research on the applications of MNWs in devices such as hard disk drive (HDD),⁵ magnetoresistive random-access memory

(MRAM),⁶⁻⁸ and GMR sensors.⁹⁻¹¹ The propagation of magnetic domain walls inside arrays of MNWs can also provide a method to store information via spintronic. 12-16 Besides memory industries, MNWs can also be applied in biomedicine. MNWs can be easily distinguished by Magnetic Resonance Imaging (MRI).¹⁷ Also, after the surfaces of MNWs are biologically functionalized with polymers, certain type of cells can be labelled by MNWs for readout and/or separation. 18,19 The heating effect of the MNWs under alternating magnetic field (AMF) enables hyperthermia treatment for the cancer and the nanowarming of cryopreserved organs.²³

The nanowarming of a cryopreserved organ is a very sensitive process and the heating rate is critical to the viability of the organ after heating. The heating rate must be above a critical warming rate for each cryoprotective agent, or devitrification will result which will damage the organ.²⁴ Heating must also be uniform, so the organ does not experience cracking.²⁵ MNWs are promising nanowarmers because they have high saturation magnetization and are small enough to distribute uniformly in the vasculature of most organs. This paper takes use of the micromagnetic simulation to find out what type of isolated MNW will best fit the requirement for the

nanowarming process of cryopreserved organs and will serve as a reference for synthesizing proper MNW arrays in experiment.

METHOD

The micromagnetic simulation tool Object Oriented Micromagnetic Framework (OOMMF)²⁶ was used to simulate single MNWs which are difficult to measure due to their small size. OOMMF uses finite element simulation where samples are subdivided into finite number of small units called meshes and the micromagnetic calculation is done for each element (mesh) before the final output is the sum of all the results in each mesh. The simulation is accomplished by solving the Landau–Lifshitz–Gilbert equations (LLG) for the system to reach equilibrium under each given condition.²⁷ In detail, the goal is to minimize the energy within the system, which is obtained by the Brown's equation:

$$M \times \mathbf{H}_{eff} = 0. \tag{1}$$

M is the magnetization of the sample. According to Landau and Lifshitz, and the damping constant α introduced by Gilbert, equation is written in the form of an ODE with respect to time:

$$\frac{dM}{dt} = -|\overline{\gamma}|M \times H_{eff} - \frac{\alpha|\overline{\gamma}|}{M_s}M \times (M \times H_{eff})$$
 (2)

where $\overline{\gamma}$ is called the Landau-Lifshitz gyromagnetic ratio.

To minimize the system energy as described above, $H_{\rm eff}$ is further defined as the summation of all the field in the system:

$$H_{eff} = H_{ext} + H_{exch} + H_{dem} + H_{anis}$$
 (3)

where constituent fields are external, exchange, demagnetization, and anisotropy of the system, respectively. The external field is input manually, similar to a hysteresis loop measurement where the applied field is swept from positive saturation to negative saturation and back. $H_{\rm dem}$ is calculated within the MNWs as:

$$H_{dem}(\mathbf{r}) = \frac{1}{4\pi} \left(-\int_{\mathbf{r}'} \frac{(\mathbf{r} - \mathbf{r}')\nabla' \cdot \mathbf{M}(\mathbf{r}')}{|\mathbf{r} - \mathbf{r}'|^3} dV' + \oint_{\mathbf{S}'} \frac{(\mathbf{r} - \mathbf{r}')\hat{\mathbf{n}} \cdot \mathbf{M}(\mathbf{r}')}{|\mathbf{r} - \mathbf{r}'|^3} dS' \right).$$

The exchange field for a ferromagnetic material is defined as:

$$H_{exch} = \frac{2A}{\mu_0 M_s^2} \nabla^2 m, \tag{5}$$

where A and M_s are the exchange coefficient and saturation magnetization that are dependent on the choice of material.

And finally, the anisotropy H_{anis} will be divided into 2 parts, the crystalline anisotropy, and the shape anisotropy, because a 3D model will be used in this research to represent the geometry of the MNWs. Again, the crystalline anisotropy is determined by the choice of material and the shape anisotropy is determined by the choice of the shape. For MNWs, their high cylindrical aspect ratio will cause the shape anisotropy to dominate this constituent. If an ellipsoidal shape is chosen to represent the MNWs, then:

$$H_{anis} = -m \cdot N_c, \tag{6}$$

where N_c is the demagnetizing factor for the ellipsoidal shape in its long axis, which is:

$$N_{c} = \frac{C_{3}}{(m^{2} - 1)} \left[\frac{m}{\sqrt{m^{2} - 1}} ln \left(m + \sqrt{m^{2} - 1} \right) - 1 \right], \tag{7}$$

where $C_3 = 4\pi$ in SI unit system and m represents the ratio between the long and short axes of the ellipsoid.²⁸

Following procedure is coded in OOMMF for this project: First, the material of the nanowire is specified by setting the saturation magnetization Ms, exchange constant A and the crystalline anisotropy K, which are unique to the material of the MNW. Next, the geometry of the sample is defined by either built-in codes for ellipsoids or by transferring a 2D experimental input image to a 3D structure and the scale of the 3rd dimension is specified using the function called image atlas. The third step is to sweep the sample between the positive and negative saturation magnetization in the direction of long axis of the wire. Finally, the simulation results are in two parts. One is the hysteresis loop revealing the important magnetic properties such as the coercivity and the remanence of the sample. The other result is the motion of the magnetic moment in the wire.

RESULTS AND DISCUSSION

Experimental measurements of MNWs typically involve large arrays, and therefore they often reveal features that are difficult to explain due to statistical shearing of features and interaction fields. Simulation results of individual MNW can be used to remove interaction field effects and reveal the magnetic properties that are affected by factors such as shape, size, and material of isolated MNWs, which are shown in the following parts. This is important for the application of nanowarming where the MNWs will be distributed at low concentration inside the cryopreservation agents.

For nickel MNWs with fixed length of 3 μ m, the coercivities are negatively correlated to the diameter of the wire, (Fig. 1(a)). This is consistent with the theory that expresses the coercivity field of the infinite long cylinder as: $h_{ci} = \frac{1.08D_0^2}{D^2}$, $D_0 = \frac{2\sqrt{A}}{M_s}$, where h_{ci} is the reduced coercivity field of a cylinder with high aspect ratio, D_0 is the fundamental unit length defined by the exchange constant A and saturation magnetization M_s of the material. The area enclosed by the hysteresis loop indicates the heating ability of the MNW. The width of the loop is determined by the coercivity of each wire and the height of the wire is the total magnetization of each isolated MNW. Although the area is positively related to the size of the MNW (Fig.1(b)), it is the smallest (30nm) MNW that will heat the best in nanowarming process. In the process of nanowarming a cryopreserved organ, the volume of MNW needed for a unit volume of sample is fixed. Therefore, the number of the smallest MNW in the sample will be the largest, which will be more likely to distribute uniformly in the sample.

When the diameter is further increased to 200 nm, in addition to a continued reduction in coercivity and remanence, a 'wasp waist' appears in the hysteresis loop, Fig. 2(a) (solid line). The reversal can be divided into three different parts showing three types of magnetic moment behaviors in the MNW (Fig.2(b)). First, since there is a large area for curling in 200nm-diameter nanowires, the magnetic

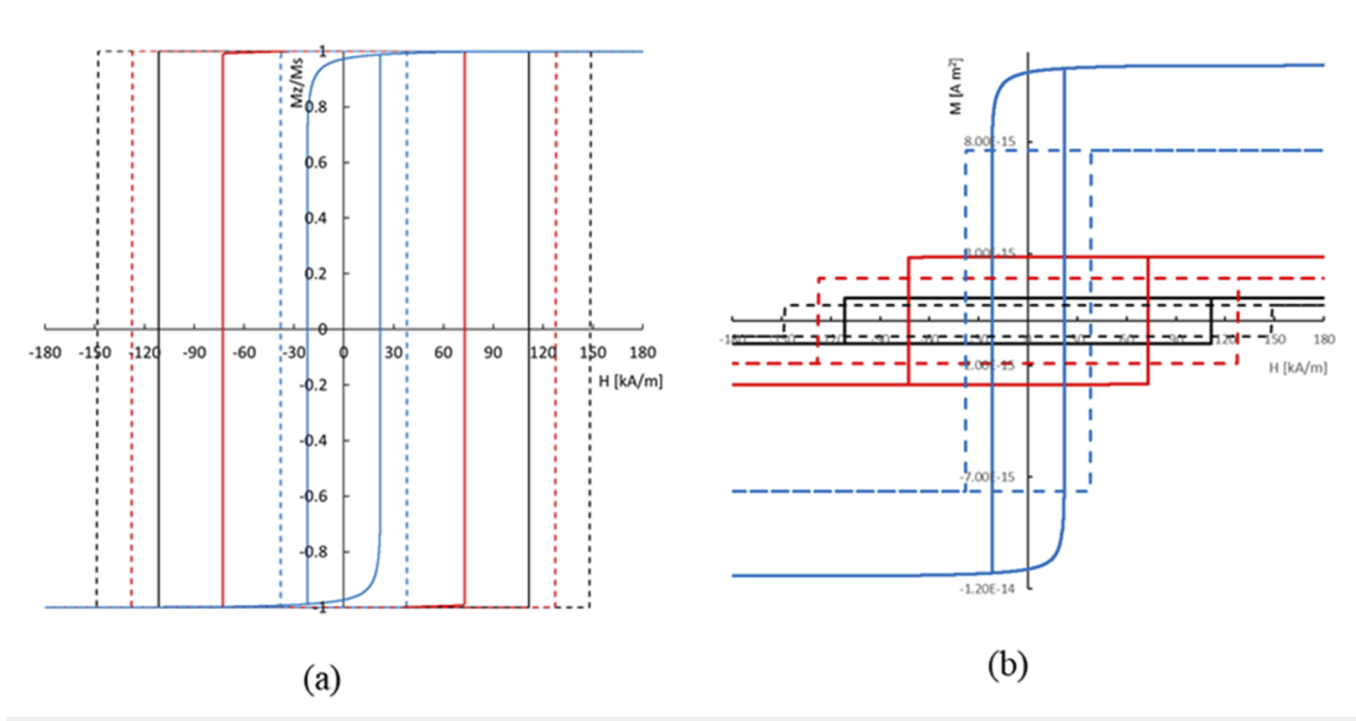


FIG. 1. A series of hysteresis loops are generated via OOMMF for nickel MNWs with diameter of 30 nm (black), 50 nm (red) and 100 nm (blue) in cylinder shape (solid line) and ellipsoid shape (dashed line). For the y-axis, normalized magnetization (a) is used to compare only the coercivity of the MNW and total magnetization (b) is used to compare the area enclosed by the hysteresis loops that represents the heating ability of a single MNW.

moments of the MNW (starting from the tips) fall from positive z direction to aligning in the xy-plane in the form of vortices as the external field starts to decrease. Next, when the external field is further reduced, the outer shell moments of MNW switch from aligning in the xy-plane to negative z direction. Finally, the axial core moments of the MNW switch to the negative z direction, and the

wire reaches full negative saturation. Interestingly, at H_c (M = 0), the two vortex walls converged at the center of the MNW, and a three-dimensional vortex (hedgehog)³⁰ is observed using the 2D cross-sectional view.

As a result, if the focus is on the vortex initially formed at the tips of the wire, it is observed that the propagation of the wall is from

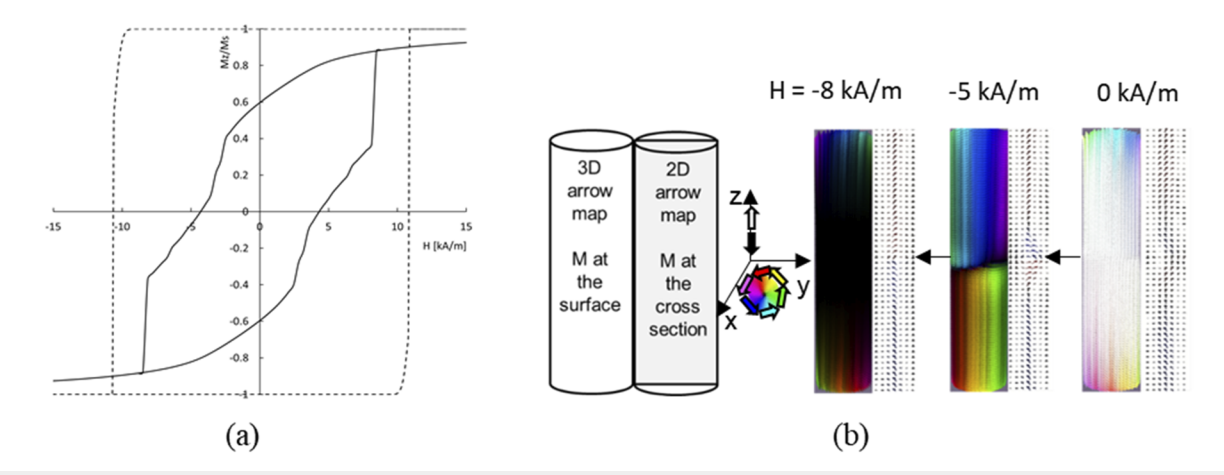
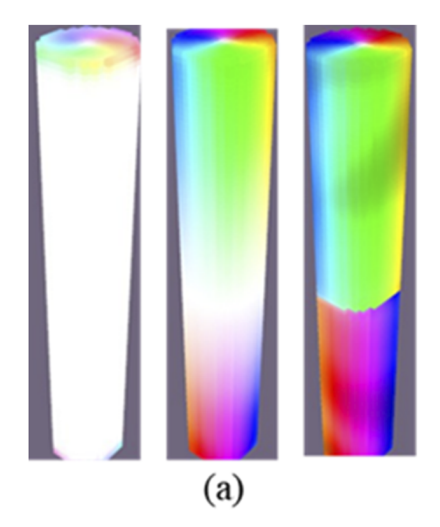


FIG. 2. (a) Hysteresis loops generated via OOMMF for 200 nm nickel MNWs with cylinder shape (solid line) and ellipsoid shape (dashed line). Numbered regions indicate the distinct periods where the domain walls exhibit different types of motion. (b) The corresponding moment state of the cylindrical wire is labelled at each chosen applied field in the form of a 3D heat map and a 2D cross section vector field.



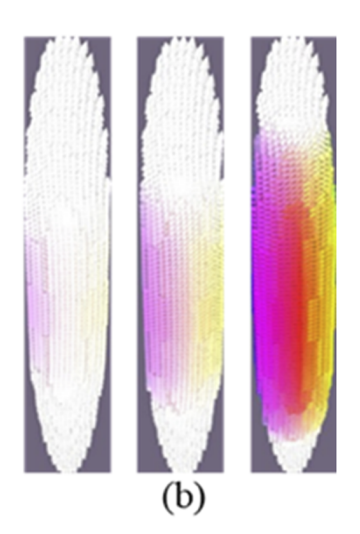


FIG. 3. States showing the different propagation patterns of the moment inside (a) cylindrical and (b) ellipsoidal 200 nm MNWs near the coercivity of the sample when the moments begin to switch direction

the two tips of the wire towards the center of the wire. Here, when all other parameters are unchanged, flat-tipped cylinders are replaced with ellipsoids so that the tips of wire have infinitesimally small areas where the curling phenomena is no longer supported. With this shape, the coercivity of the nanowires significantly increases (Fig.1 and 2(a), dashed line) to Hc = 143, 127, 40, 9 kA/m from 111, 72, 24, 4 kA/m for the MNWs with 30, 50, 100, 200nm diameters, respectively. This increase in coercivity occurs because the field to nucleate a vortex domain wall at the tips is lower than to nucleate vortex domain in the center of the wire which is the case for ellipsoidal MNWs. For these ellipsoids, increasingly negative applied fields cause the vortex to expand to include the coherent curling of the whole nanowire. The different moment states in Fig. 3 shows the difference of how the moments propagate through the wire when different shapes are designated.

As shown in Fig.2, the vortex of cylindrical 200 nm MNW begins to form before 0 kA/m. But the vortex of its ellipsoidal equivalent only begins to form at a higher external field (10 kA/m). This demonstrates the importance of MNW shape for nanowarming.

CONCLUSION

With the help of micromagnetic simulation, we are able to unveil that factors such as the size and shape are affecting the magnetic properties of isolated MNW as follows. First, if the length of the wire is fixed, the coercivity is reduced by increasing the diameter of the wire. Second, when the tip of the wire is engineered so that the nanowires are ellipsoidal rather than cylindrical, the coercivity is increased and the moment switching begins at the center of the wire instead of the end. This trend helps to find that the 30 nm isolated ellipsoidal MNWs are the optimal ones to warm up the cryopreserved organs both rapidly and uniformly based on the area of the hysteresis loop and size of the individual MNW. Importantly, although the switching pattern of 200 nm cylindrical MNWs is not good for nanowarming, the observed formation of skyrmion line and the stable hedgehog moment state during the reversal can trigger promising application in memory storage and quantum computing related area. In the future, the finding via simulation in this paper

will be extended from isolated MNW to arrays of MNWs to mimic the more realistic situation and guide the experimental synthesis of MNW.

DATA AVAILABILITY

The data that support the findings of this study are available from the corresponding author upon reasonable request.

REFERENCES

- ¹A. Fert and L. Piraux, "Magnetic nanowires," Journal of Magnetism and Magnetic Materials **200**(1-3), 338-358 (1999).
- ²L. Piraux *et al.*, "Giant magnetoresistance in magnetic multilayered nanowires," Applied Physics Letters **65**(19), 2484–2486 (1994).
- ³ A. Blondel *et al.*, "Giant magnetoresistance of nanowires of multilayers," Applied Physics Letters **65**(23), 3019–3021 (1994).
- ⁴K. Liu *et al.*, "Perpendicular giant magnetoresistance of multilayered Co/Cu nanowires," Physical Review B 51(11), 7381 (1995).
- ⁵J. Dedrick and K. L. Kraemer, "Who captures value from science-based innovation? The distribution of benefits from GMR in the hard disk drive industry," Research Policy 44(8), 1615–1628 (2015).
- ⁶M. M. Maqableh *et al.*, "CPP GMR through nanowires," IEEE Transactions on Magnetics **48**(5), 1744–1750 (2012).
- ⁷X. Huang *et al.*, "Magnetoresistance and spin transfer torque in electrodeposited Co/Cu multilayered nanowire arrays with small diameters," Journal of Applied Physics **105**(7), 07D128 (2009).
- ⁸S. Z. Rahaman *et al.*, "Pulse-width and temperature effect on the switching behavior of an etch-stop-on-MgO-barrier spin-orbit torque MRAM cell," IEEE Electron Device Letters **39**(9), 1306–1309 (2018).
- ⁹P. D. McGary *et al.*, "Magnetic nanowires for acoustic sensors," Journal of Applied Physics **99**(8), 08B310 (2006).
- ¹⁰I. Enculescu *et al.*, "Current perpendicular to plane single-nanowire GMR sensor," Applied Physics A 86(1), 43–47 (2007).
- ¹¹B. Cox, D. Davis, and N. Crews, "Creating magnetic field sensors from GMR nanowire networks," Sensors and Actuators A: Physical 203, 335–340 (2013).
- ¹²G. Hrkac, J. Dean, and D. A. Allwood, "Nanowire spintronics for storage class memories and logic," Philosophical Transactions of the Royal Society A: Mathematical, Physical and Engineering Sciences 369(1948), 3214–3228 (2011).
- ¹³S. Bhatti *et al.*, "Spintronics based random access memory: A review," Materials Today **20**(9), 530–548 (2017).

- ¹⁴M. V. Puydinger dos Santos *et al.*, "Annealed cobalt–carbon nanocomposites for room-temperature spintronic applications," ACS Applied Nano Materials 3(7), 7143–7151 (2020).
- 15 L. Galdun *et al.*, "High spin polarization in Co $_2$ FeSn Heusler nanowires for spintronics," ACS Applied Nano Materials 3(8), 7438–7445 (2020).
- ¹⁶ L. Siemer, I. Ovsyannikov, and J. D. M. Rademacher, "Inhomogeneous domain walls in spintronic nanowires," Nonlinearity 33(6), 2905 (2020).
- ¹⁷D. Shore *et al.*, "Electrodeposited Fe and Fe-Au nanowires as MRI contrast agents," Chemical Communications **52**(85), 12634–12637 (2016).
- ¹⁸W. Zhou et al., "Development of a biolabeling system using ferromagnetic nanowires," IEEE Journal of Electromagnetics, RF and Microwaves in Medicine and Biology 3(2), 134–142 (2018).
- ¹⁹M. R. Zamani Kouhpanji, J. Um, and B. J. H. Stadler, "Demultiplexing of magnetic nanowires with overlapping signatures for tagged biological species," ACS Applied Nano Materials 3(3), 3080–3087 (2020).
- ²⁰D. S. Choi *et al.*, "Hyperthermia with magnetic nanowires for inactivating living cells," Journal of Nanoscience and Nanotechnology **8**(5), 2323–2327 (2008).
- ²¹ J. Alonso *et al.*, "FeCo nanowires with enhanced heating powers and controllable dimensions for magnetic hyperthermia," Journal of Applied Physics **117**(17), 17D113 (2015).

- ²²P. W. Egolf *et al.*, "Hyperthermia with rotating magnetic nanowires inducing heat into tumor by fluid friction," Journal of Applied Physics **120**(6), 064304 (2016).
- ²³ Z. Gao, B. Namsrai, Z. Han, P. Joshi, J. S. Rao, V. Ravikumar, A. Sharma et al., "Vitrification and rewarming of magnetic nanoparticle-loaded rat hearts," Advanced Materials Technologies, 2100873 (2021).
- ²⁴D. Shore *et al.*, "Nanowarming using Au-tipped Co₃₅Fe₆₅ ferromagnetic nanowires," Nanoscale 11(31), 14607–14615 (2019).
- ²⁵ A. Sharma, J. S. Rao, Z. Han, L. Gangwar, B. Namsrai, Z. Gao, H. L. Ring et al., "Vitrification and nanowarming of kidneys," Advanced Science 8, 2101691 (2021).
- ²⁶M. J. Donahue and M. J. Donahue, OOMMF User's Guide, Version 1.0, U.S. Department of Commerce National Institute of Standards and Technology, 1999.
- ²⁷D. Kumar and A. O. Adeyeye, "Techniques in micromagnetic simulation and analysis," Journal of Physics D: Applied Physics 50(34), 343001 (2017).
- ²⁸ B. D. Cullity and C. D. Graham. *Introduction to Magnetic Materials* (John Wiley & Sons, 2011).
- 29 S. Madhukar Reddy *et al.*, "Magnetization reversal mechanisms in 35-nm diameter Fe_{1-x}Ga_x/Cu multilayered nanowires," Journal of Applied Physics **111**(7), 07A920 (2012).
- ³⁰ Magnetic Nano- and Microwires: Design, Synthesis, Properties and Applications, edited by M. Vázquez (Woodhead Publishing, 2015).